Theoretical investigation into the feasibility to deposit RF energy centrally in the head and neck region.

M.M. Paulides[1], S.H.J.A. Vossen[2], A.P.M. Zwamborn[2], G.C. van Rhoon[1].

[1] Erasmus MC - Daniel den Hoed Cancer Center,
Department of Radiation Oncology, Section Hyperthermia
PO box 5201, NL-3008 AE, Rotterdam, The Netherlands
Tel.no. : +31 10 4391676
Fax.no. : +31 10 4391022
E-mail: M.Paulides@ErasmusMC.nl

[2] The Netherlands Institute for Applied Scientific Research (TNO),
The Hague, The Netherlands

August 23, 2007

Running title: "Parameter investigation into heating neck tumours"

Abstract

Purpose: *Investigation of the ability to deposit radiofrequency (RF) energy centrally in the neck as a function of antenna positions, number of antennas and operating frequency.* ***Materials and methods:*** *Power absorption (PA) distributions in a realistic model of the head and neck anatomy are calculated, where the head model is irradiated by an array of dipole antennas. The relative PA distributions corresponding to different set-ups are visualized and analyzed using the ratio of the average PA (aPA) in the target and neck region.* ***Results:*** *Both the PA distributions and aPA ratios indicate an optimal focussing ability of the set-ups, i.e. the ability to direct energy efficiently into the target region, between 400 and 600 MHz. In this frequency band the focussing ability depends only moderately on the size of the neck. Finally it is found that the focussing ability at 433 MHz is increased significantly by increasing the number of antenna elements.* ***Conclusions:*** *The optimal frequency is found to be highly dependent on the size of the target volume; thus a single optimum is hard to define. However, future clinical research will focus on 433 MHz based upon the optimal range of frequencies, as found in this study.*

1 Introduction

Patients with advanced carcinomas in the head and neck (H&N) have a dismal prognosis. Locoregional control still poses a major therapeutic challenge. For tumours considered to be unresectable, the traditional treatment has been conventional fractionated radiotherapy (RT) resulting in low 2-year survival rates (30%) for stage III/IV disease[1,2]. Introducing hyperfractionation and/or accelerated radiation treatment schedules have substantially improved the poor treatment outcome[3–5]. Similarly, by combining RT with simultaneous chemotherapy an 8% increase of overall 2-year survival was reported in the three meta-analyzes study of Pignon *et al.*[6]. Unfortunately, the improved treatment outcome is at the cost of increased toxicity[7], in particular of the mucosal linings[8], where for older patients this treatment is even too toxic. Consensus exists that the optimal strategy for treatment of advanced unresectable H&N carcinomas remains to be defined and that the identification of a combined modality treatment with equal or better treatment outcome but with a lower toxicity is of high priority.

New strategies currently under investigation, like ARCON, hypoxic cell sensitizers and angiogenesis, focus on killing the radioresistant, hypoxic tumour cell population[9]. Some of these approaches have shown improved treatment outcome but have not gained general acceptance. The unique feature of HT is that it enhances local tumour control but it does not increase radiation toxicity[10]. From the perspective of the focus on the radioresistant hypoxic cell population it is disappointing that the potential of hyperthermia (HT) to greatly enhance the local control (from 24% for RT alone to 69% for RT + HT) and survival rate (from 0% for RT alone to 50% for RT + HT) for metastatic lymph nodes in Stage IV carcinoma of the H&N without additional toxicity, as was demonstrated in a phase III study by Valdagni *et al.*[11,12], has not been further explored.

In 1997 Amichetti *et al.*[13] showed that HT also improves treatment outcome when added to a hyperfractionated radiation schedule, but does not increase toxicity.

In our opinion a major cause of the loss of interest in the combined treatment of RT+HT for advanced H&N tumours has been the lack of a good HT system to adequately heat tumours at this location. HT treatment of H&N tumours involves the heating of tumour tissue extending from the surface to as deep as the center of the neck, e.g. depths from 0 to 7 cm. From our own clinical experience (unpublished data) we know that in general cervical lymph nodes can be heated relatively easy with electromagnetic (EM)-energy, but that it is much more difficult to adequately heat the more deeper located tumours. The latter is confirmed by the experiences of other HT groups. Serin *et al.*[14] reported adequate ability to heat superficial metastatic cervical lymph nodes using a commercial ultrasound (US) system, though nodal volume and depth influence the quality of the heating. Wust *et al.*[15] and Ben-Yosef and Kapp[16] compared the performance of heating of more deeply located H&N tumours, e.g. surrounded by bone and air, using EM or US technology. They reported that HT applied by US was limited by bone pain and showed inferior temperature distributions in comparison to heat applied by single EM applicator systems. Wust *et al.*[15] anticipate that the use of a specific designed HT applicator consisting of an array of EM antenna elements will result in large improvements in the quality of heating advanced H&N tumours.

Overall, the great potential of combined RT+HT for the treatment of advanced H&N tumours in combination with the significant progress in radiofrequency (RF) applicator technology as well as in EM modeling, is a strong stimulant for us to start the development of a site-specific EM applicator system for HT treatment of H&N tumours. In this paper we report on the results of a theoretical study into the feasibility of such an applicator system where the focus is on the arrangement of antenna elements and the optimal frequency for heating tumours located in the neck region. An important criterion for the frequency selection is our demand that the applicator must have the flexibility to heat both advanced laterally located tumours and tumours located at the midline of the H&N region. Hence, the power absorption (PA) distribution must be controlled in both the axial and radial direction for which amplitude and phase steering is essential. Axial PA control requires multiple antenna rings whereas control of the radial PA distribution is obtained by placing multiple antennas in a circular array configuration. The ability to obtain a high PA at the center of the neck will be the most challenging and difficult problem to solve because penetration depth is strongly frequency dependent[17]. Therefore, in this study, we have focussed on investigating the dependence of the PA at the center of the neck as the complex function of number of EM-sources in one ring and frequency.

2 Materials and methods

Investigation of all parameters and their combined effects requires a huge amount of calculations. Therefore, this numerical investigation is split into three series of calculations. The first series of calculations addresses the influence of the placement and number of antennas for a rough selection of frequencies using one patient. The parameter under investigation for the second series of

calculations is the operating frequency while using the number of antenna elements that offers a good discrimination between the results obtained at these frequencies. A single optimal frequency is will be hard to find since the absorbed power is to a large extent dependent on the size of the area that should be treated. Hence, in addition to the frequency investigation for a target volume of 5x5x5 cm we also varied the target size in the analysis. Finally, for the last (third) series of calculations, we scaled the patient anatomy obtaining three set-ups: a small, average (1.24x) and large (1.39x) anatomy, where the diameter of the neck is 9.7, 12 and 13.5 cm, respectively. For these configurations a constant number of antennas is used (eight) and a constant antenna-tissue distance is applied. This part is mainly dedicated to the need for a high penetration depth and focuses on frequencies within the frequencyband, as selected from the second series of calculations.

2.1 Anatomy model

The entire volume is divided into a finite number of volume elements, e.g. voxels, for use in numerical calculations with a computer program. Assigning tissues to these voxels results in a head segmentation.

For the first step of the head segmentation process we used a CT-scan of a H&N RT patient consisting of 69 transverse 2-D CT-slices. A 3-D model of the head and neck region is constructed automatically from these 2-D slices by a dedicated computer program. In this model, four different regions of Hounsfield values are defined and labelled automatically, which leads to a rough head segmentation. Subsequently, organs are assigned manually. For the analysis we introduce a hypothetical target volume with realistic content in the model at the central neck location.

The head model is truncated at the level of the shoulders and nose and no matching at the transition to the water is applied because it is assumed that the distance to the area of interest was sufficient to suppress the influences of reflections. Each voxel measures 2.83, 2.83, 2.50 mm in dimension (x, y and z-axis), where the geometrical dimensions of the head model are 234, 424 and 173 mm, respectively. The diameter of the neck of this particular example patient is found to be relatively small[18] i.e. 9.7 cm. The influence of larger necks is investigated by using two scaled versions of this H&N model. Scaling was carried out to obtain H&N models with neck diameter of 12.0 and 13.5 cm, respectively. Note that this scaling implies multiplication of the voxel sizes with an equal scalar in all Cartesian directions.

Figure 1 shows transversal and sagittal cross-sections of the tissue distribution in the model, where the tissue coding is according to Table 1. The cross-sections through $z = 0$ mm and $y = 14$ mm have been chosen to visualize the results avoiding inclusion of the trachea where the PA results will be equal to zero since the trachea is a non-conducting material. Note that the single dark spots at the edges of the anatomy represent wet skin (11) and not perfectly electric conducting (PEC) material.

2.2 Applicator model

The use of dipole antennas within a clinical environment is common. Consequently, dipoles are used as radiating elements in our study. Calculations are carried out with one, four, six, eight or 16

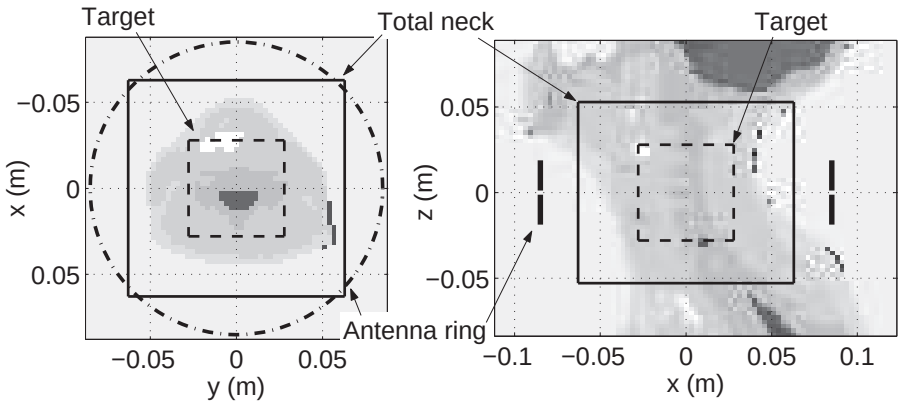

Figure 1: Tissue distribution in the neck and positioning of the antennas around the neck at cross-sections through (a) $z = 0$ mm and (b) $y = 14$ mm. The tissue type index (tti) values correspond with those in Table 1.

Table 1: Dielectric properties of the tissue types at 100, 433 and 915 MHz ($\mu_r = 1.0$).

Tissue type (index)	100 MHz		433 MHz		915 MHz	
	ϵ_r [-]	σ [S/m]	ϵ_r [-]	σ [S/m]	ϵ_r [-]	σ [S/m]
0. De-ionised water	78	$2*10^{-3}$	78	0.04	78	0.18
1. Trachea	10	0.00	1	0.00	1	0.00
2. Fat	6	0.04	6	0.04	6	0.05
3. Muscle	66	0.71	57	0.81	55	0.95
4. BoneCortical	15	0.06	13	0.09	12	0.15
5. Air bubble	1	0.00	1	0.00	1	0.00
6. Lung	1	0.00	1	0.00	1	0.00
7. Tooth	15	0.06	13	0.09	12	0.15
8. Cartilage	56	0.48	45	0.60	43	0.79
9. BrainGrey matter	80	0.56	57	0.75	53	0.95
10. BrainWhite matter	57	0.32	42	0.45	39	0.60
11. SkinWet	66	0.52	46	0.68	46	0.85
12. Gland	69	0.80	61	0.89	60	1.04
13. PEC	1	$1*10^6$	1	$1*10^6$	1	$1*10^6$

dipole antennas embedded in de-ionized water. Equal spacings between the antennas are used since according to Henke *et al.*[19] a symmetrical array performs best for a symmetrical set-up, which is approximately the case for the neck region. The operating frequency is chosen from the interval of 100 to 915 MHz which includes the entire region indicated for this site[20], i.e. between 100 and

750 MHz, and the closest ISM[1] frequencies. The dipole antennas are equally-spaced positioned on a, 170 mm in diameter, circle that surrounds the neck ("Antenna ring": Figure 1). The diameter of the antenna ring is increased for the scaled model in order to keep a constant distance between the antennas and the skin of the patient for all set-ups, i.e. the diameters for these set-ups are 193 and 208 mm. The sources are of equal phase and amplitude since this is expected to result in positive interference in the central region. Phase and amplitude optimization has been omitted in the entire study. The length of the dipole antennas (L_{dip}) is chosen such that they are resonant or smaller since this provides equal radiation patterns[21], i.e. 3.75 cm for low frequencies (f = 433 MHz) and 1.75 cm for higher frequencies ($f >$ 433 MHz) are used. An infinite de-ionized water environment with a relative permittivity of 78.0 is used as waterbolus since the influences of a waterbolus are not subject of this study.

2.3 Electromagnetic modelling

A finite-difference time-domain (FDTD) based program[2 22] is used to calculate the PA distributions. The FDTD algorithm is widely used and described extensively, e.g. by Taflove[23]. The algorithm calculates the electric (E) and magnetic (H) fields in a discrete space and time frame. The PA value in a certain voxel is obtained from the electric field components at every point:

$$\mathrm{PA} = \frac{\sigma_{eff}|\vec{E}|^2}{2} \quad (Wm^{-3}) \tag{1}$$

where σ_{eff} is the effective conductivity (S/m). Note that the PA values differ only by the tissue-dependent mass density from the specific absorption rate (SAR) values. As main inputs, the program requires the head model and an applicator model. Mur's second-order absorbing-boundary conditions (ABC)[24] are applied to terminate the borders of the entire computational domain. A uniform rectilinear mesh is used and additional voxels between the head model and ABC are applied to reduce the influence of reflections at the ABC's. For high frequencies ($f \geq$ 433 MHz) the computational domain consists of 163, 170 and 89 voxels (= 2.5 million voxels) in the x, y and z-direction respectively, where the dimensions of a voxel are 2.9, 2.9 and 2.5 mm. For low frequencies ($f <$ 433 MHz) the domain is extended with 10 voxels in all directions since the penetration depth in water is higher at these frequencies. The dielectric properties of the tissues per frequency are found using an application of IFAC-CNR[25] based on a parametric model by Gabriel *et al.*[26]. As an example the dielectric properties at 100, 433 and 915 MHz are given in Table 1, where isotropic tissues are assumed. The dielectric properties of the trachea and lung are chosen equal to those of air since from the results of Gabriel it was not clear whether the entire lung and trachea were considered or just the organ walls. The properties of de-ionized water (salinity = 0.00 g/l, T = 20°C) and PEC are assumed to be dispersion-free. The dipoles of the applicator are approximated by so called "hard sources"[23], i.e. electric-field point sources, that excite two conducting wires (PEC material, Table 1) with a cross-section of 2.89 x 2.89 mm2.

[1] ISM frequencies: these are frequencies allocated for applications in Industry, Science and Medicine. In most European countries they are: 27.12, 433 and 2450 MHz. In the USA 433 MHz is replaced by 915 MHz.

[2] FDTD program developed at TNO-FEL, The Hague, The Netherlands.

2.4 Evaluation

The evaluation of the PA distributions is carried out qualitatively by comparing visualizations of cross-sections trough the PA distribution at $z = 0$ mm and $y = 14$ mm. The distributions are normalized to the average PA value in the neck region ($\mathrm{PA}_{\text{neck volume}}$): $\mathrm{PA}_{\text{norm}}(\mathrm{x,y,z}) = \mathrm{PA(x,y,z)}/\mathrm{PA}_{\text{neck volume}}$. Visualization of the PA distribution by color plots is strongly influenced by the choice of the normalization method. This makes it difficult to evaluate the treatment quality from these visualizations alone. As our aim was to assess the ability of a set-up to direct power to the central target region we selected the average power absorption ratio to quantify the relative amount of energy that is absorbed in the target region. It is defined as:

$$\text{aPA ratio} = \frac{\sum_{\text{target volume}} \frac{\mathrm{PA}(x,y,z)}{N_{\text{target volume}}}}{\sum_{\text{neck volume}} \frac{\mathrm{PA}(x,y,z)}{N_{\text{neck volume}}}}$$

where $\mathrm{N}_{\text{neck volume}}$ and $\mathrm{N}_{\text{target volume}}$ are the total amount of tissue voxels in the neck and target volume, respectively. This ratio is found to depend little on the size of the neck volume but to a large amount on the dimensions of the target volume. The neck volume is defined as the tissue voxels within a 12x12x10 cm brick volume (Figure 1). We chose to use a target volume of 5x5x5 cm because the aim is to treat advanced tumours. However, since the aPA ratio is highly dependent on the target size, other target volume dimensions are shown as well. The target volume dimensions range from 2x2x2 cm (8 cm^3) to 8x8x8 cm (512 cm^3) since the aim is on treating all from a primary tumour up to a combination of a large primary tumour and/or its lymph node metastases.

3 Results

3.1 Positioning and optimal number of dipoles in a single antenna ring

The first series of calculations are carried out using 1, 4, 6, 8 and 16 antennas at 100, 433 and 915 MHz. Concerning the positioning of applicator sources it is found that the PA distributions are influenced adversely by a region of high PA at the chin, due to the local irregular tissue distribution. Therefore, all set-ups are rotated such that the antenna-chin distance is as large as possible to circumvent this problem, e.g. for eight antennas a 22.5° rotation is applied with respect to the 0° position in front of the chin (Figure 2a-c).

Figure 2 shows the normalized PA distributions for four, eight and sixteen dipoles around the neck at a cross-section through the sources of the dipoles. The positions of the dipoles are visible by the white spots indicating local very high PA values due to a high imposed electric field. The central target region and neck region are indicated by the white squares. Figure 2a shows that the interference pattern at 433 MHz of four dipoles does not fulfill the requirements to direct the energy specifically to the central region. A much more pronounced focal area, i.e. a region of high PA, is obtained when using eight (Figure 2b) or sixteen sources (Figure 2c), where little difference is visible between eight and sixteen dipoles. Figure 3 shows the aPA ratio results at 100, 433 and 915 MHz for the various set-ups with different number of radiating elements. It is found that the highest aPA ratio values are obtained using 433 MHz with sixteen dipoles but the plateau starts

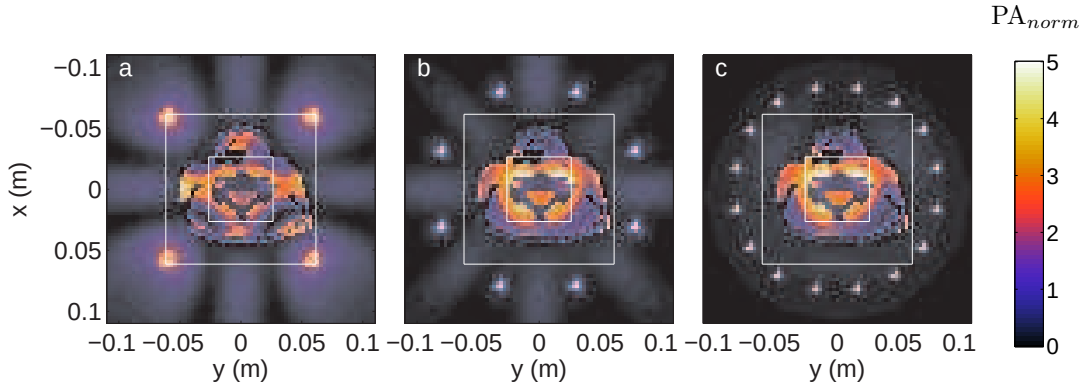

Figure 2: PA distributions in the neck at cross-sections through $z = 0$ resulting from FDTD calculations with 433 MHz for a) 4, b) 8 and c) 16 dipole antennas. The PA values are normalized to the average value in the neck volume. The target and neck volume are indicated by the white squares.

roughly at eight dipoles. The curves corresponding to 100 and 433 MHz show a similar behavior. The curve belonging to 915 MHz, however, shows a decreased aPA ratio for six antennas. This is the result of secondary foci (foci other than the central focus) that are present in the tissue at this frequency. Based on these results we chose to use eight dipoles since this number of antennas provides the best compromise between the constraint to use as few antennas as possible and best performance in terms of aPA ratio.

3.2 Optimum operating frequency

The second series of PA predictions is performed to study the influence of the frequency on the ability to heat centrally located target volumes of various sizes. Figure 4 shows the PA distributions for all frequencies under consideration using an eight dipole configuration. It is observed that low frequencies (100 MHz and 144 MHz) result in superficial absorption only, whereas the antenna set-up performs insufficient at high frequencies (700 MHz and 915 MHz) due to secondary in tissue. Multiple foci in the surroundings, besides in the target volume, lead to unwanted high superficial PA. Also, the high frequencies lead to high PA values in the surrounding water and consequently to high losses which reduces the efficiency of the applicator. Unwanted high PA values are visible in the chin region as well, for high and low frequencies, due to a lower central PA intensity. Note that for high frequencies smaller dipoles are used and thus the antenna-chin distance is larger, which implies that the PA in the chin was expected to be lower. The intermediate frequencies result in a centrally positioned focus covering almost the entire target domain. As expected, the bony structures receive little energy due to their low conductivity.

Figure 5 summarizes the PA distributions of Figure 4 by displaying the corresponding aPA ratio values: as a function of target volume and frequency. It shows that the antenna set-up performs well in the range of frequencies between 300 MHz and 700 MHz, where the optimum depends on the target size. When we focus towards the most likely target volume sizes (4x4x4 cm to 6x6x6 cm),

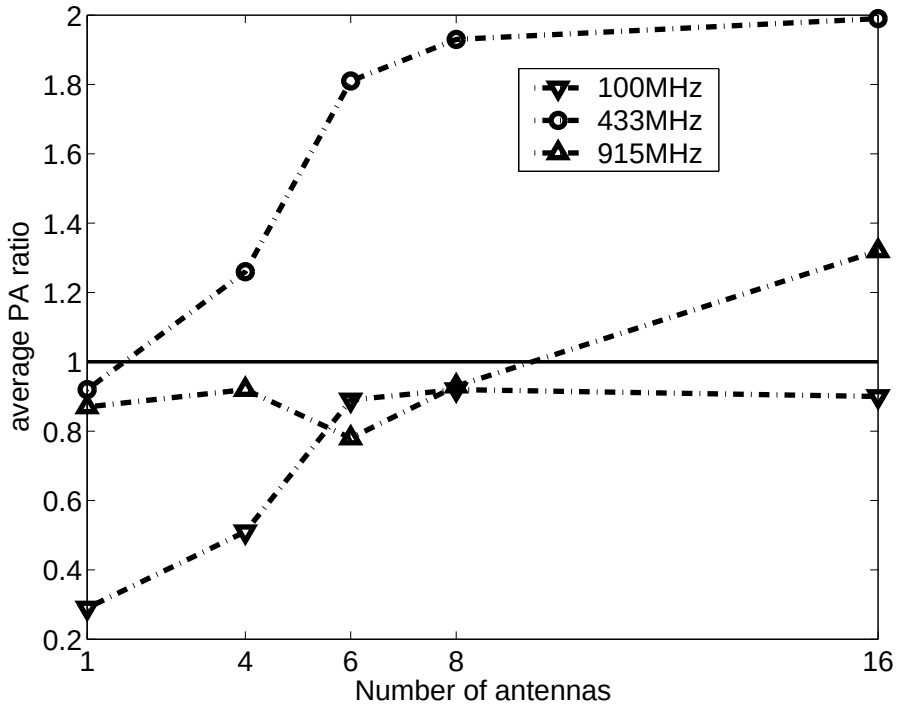

Figure 3: aPA ratio values as a function of number of sources for 100 MHz, 433 MHz and 915 MHz. The target volume is 5x5x5 cm and the neck volume 12x12x12 cm.

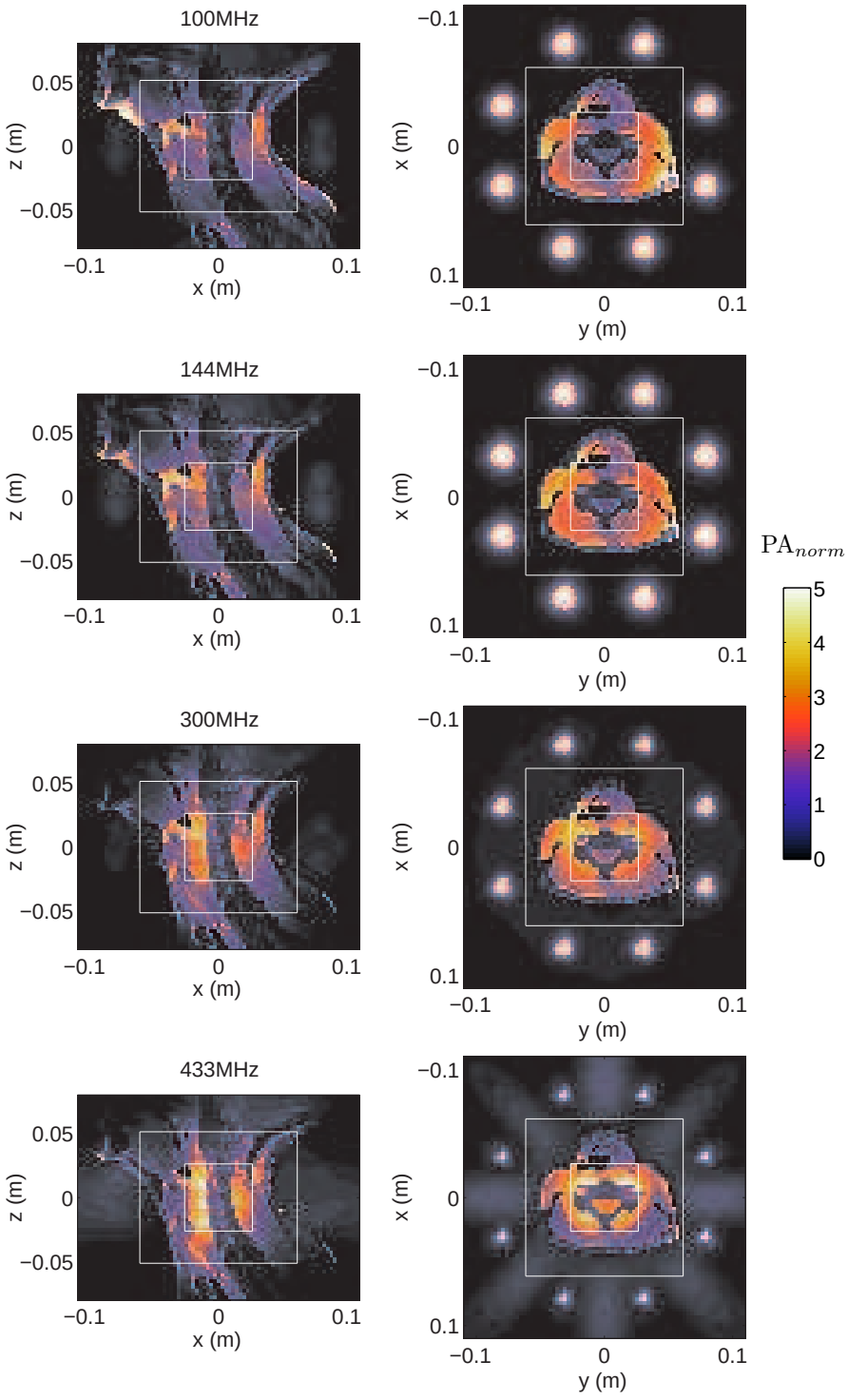
100MHz
144MHz
300MHz
433MHz
z (m)
x (m)
y (m)
0.05
0
−0.05
−0.1
0.1
PA$_{norm}$
5
4
3
2
1
0

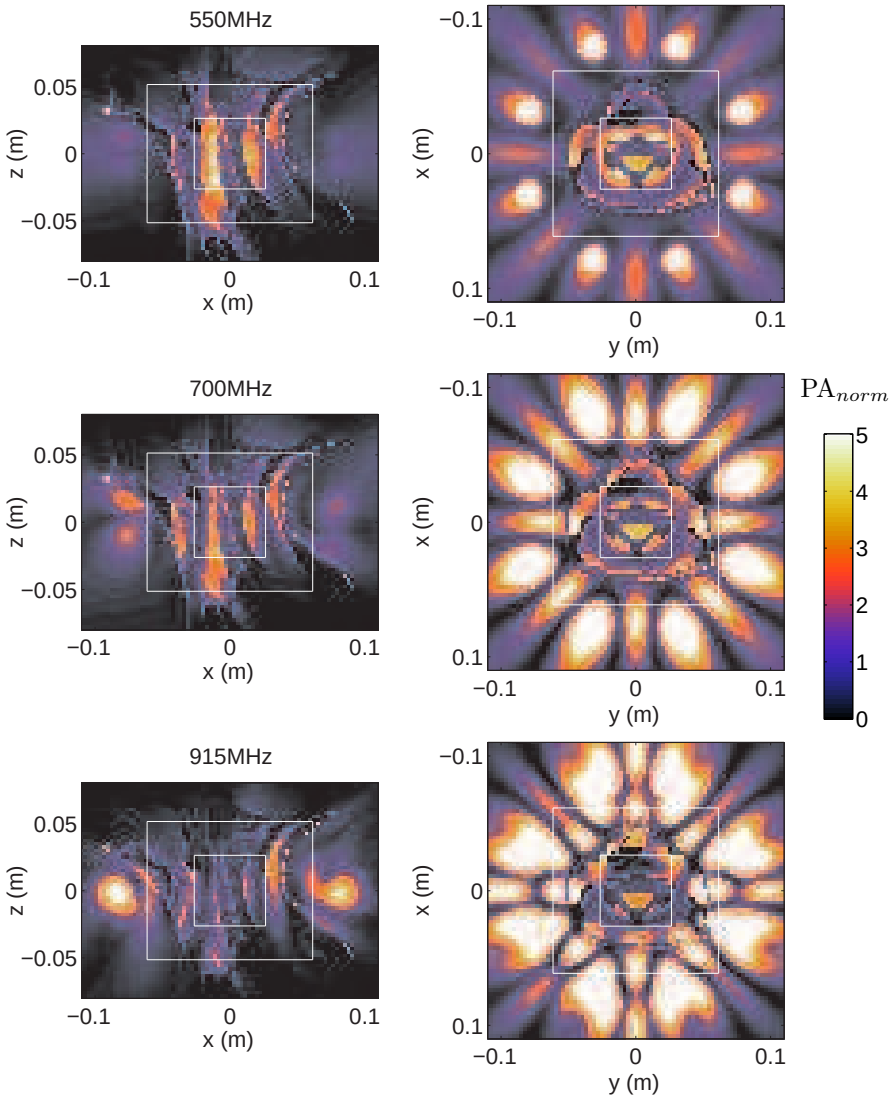

Figure 4: PA distributions in the neck at cross-sections through $y = 14$ mm (left) and $z = 0$ mm (right) resulting from FDTD calculations. The PA values are normalized to the average value in the neck volume. The target and neck volume are indicated by the white squares.

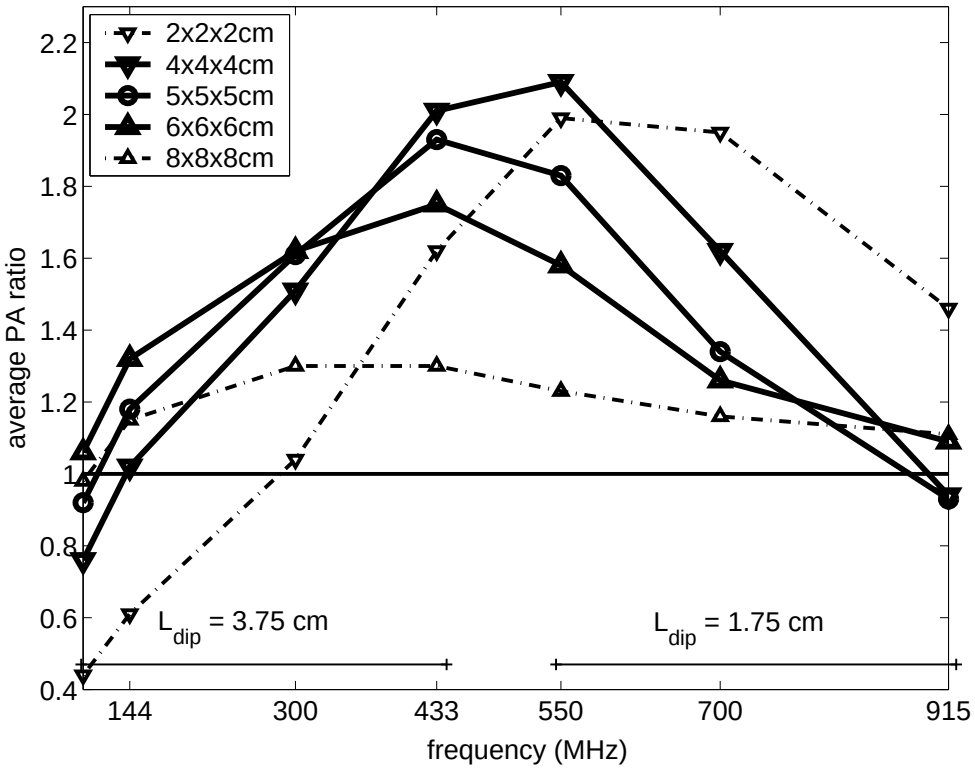

Figure 5: aPA ratio values calculated with FDTD as a function of frequency for different target volume sizes. aPA = 1, i.e. the average PA in target and neck volume are equal, is indicated.

this range of optimal frequencies decreases to frequencies between 400 MHz and 600 MHz. For the latter frequencies the average PA in the target volume is approximately two-fold the average PA in the neck volume. Note that higher frequencies perform best for small target volumes and lower frequencies perform marginally better for large target volumes. Note further that the sensitivity of the performance of the system as a function of the frequency is high for small, but low for large target volumes.

3.3 Influence of the neck dimensions on the frequency

The third and last series of calculations are carried out to investigate the dependence on the aPA curve of the neck dimensions. Frequencies in the most suitable range for this application are used for this investigation, i.e. 300, 433 and 550 MHz. The distances between the antennas and the skin are constant for all set-ups.

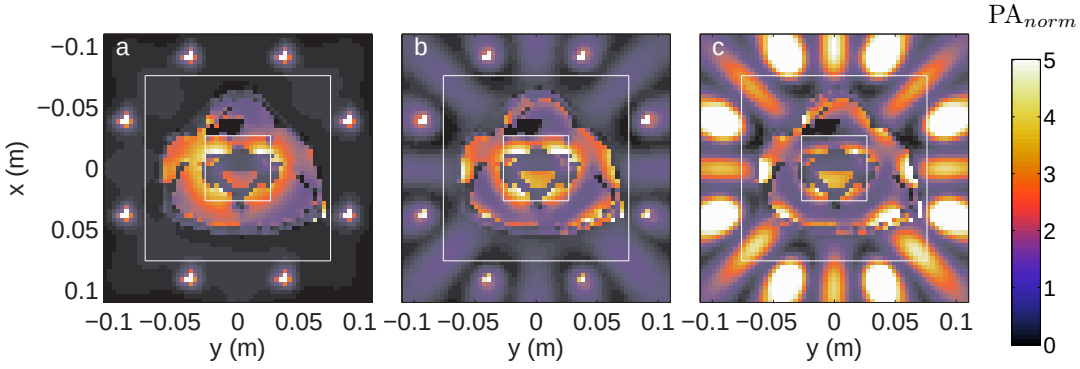

Figure 6: PA distributions in the average neck at cross-sections through $z = 0$ resulting from FDTD calculations at a) 300, b) 433 and c) 550 MHz for 8 dipole antennas. The anatomy is scaled with a factor 1.24 (= 12.0 / 9.7) with respect to the original head and neck model. The PA values are normalized to the average value in the neck volume. The target and neck volume are indicated by the white squares.

Figure 6 shows the PA distributions for an average anatomy and an eight dipoles configuration operating at 300, 433 and 550 MHz. For comparison reasons the neck and target region (white squares) are equal for all set-ups and equal to the situation for a small neck. Figure 6 shows similar distributions, for the average neck, compared to a small patient: comparing this figure to Figure 4 (300, 433 and 550 MHz) reveals that the overall pattern remains intact for this larger patient but the superficial absorption increases. This effect is most pronounced at 550 MHz due to the nearby secondary foci.

Figure 7 provides a summary in terms of aPA ratio of figure 6 for the small, average and large patient anatomy. It reveals that a large diameter of the neck has a negative influence on the PA pattern at 550 MHz, i.e. the aPA ratio decreases. Further it shows that an increase in anatomy size advocates a lower operating frequency. The analysis shows that 433 MHz from the available

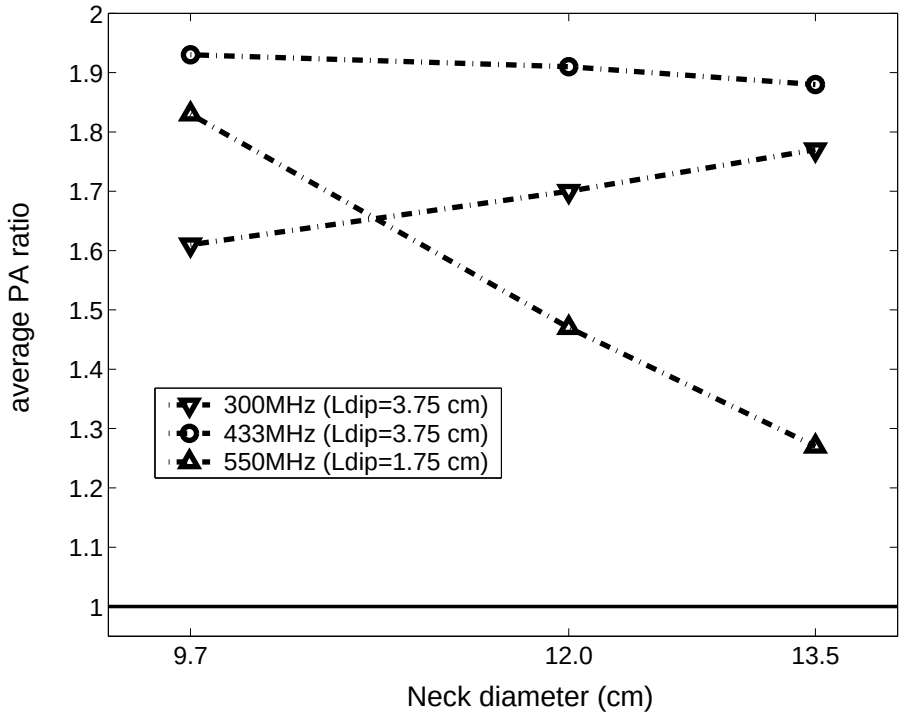

Figure 7: aPA ratio values calculated with FDTD as a function of frequency for an anatomy with a small, average and large neck diameter. The target region is 5x5x5 cm and the neck volume is 12x12x10 cm, 14.8x14.8x12.4 cm and 16.7x16.7x14.0 cm for the small, average and large configuration, respectively.

frequencies and studied configurations 433 MHz performs best in all cases.

4 Discussion

4.1 Evaluation of the materials and methods

In work published by Jacobson and Melandsø[20], a possible frequency range of 100 to 750 MHz is indicated for heating H&N tumours. Taking into account the results of their 20 study we selected the frequencies that are used in this study. The three frequencies that are selected for the determination of a suitable number of antennas, i.e. 100 MHz, 433 MHz and 915 MHz, span the indicated frequency interval and/or conform to ISM frequencies. For the first two frequencies high-power amplifiers are available in our department (Erasmus MC - Daniel den Hoed Cancer Center) enabling future verification PA measurements in phantom models.

The first part of this work is the construction of a (truncated) anatomy segmentation. The truncations have little influence on the PA distribution in the neck volume because the electric field near the transitions is low; thus little power is reflected at the boundaries.

To reduce the number of set-ups to be analyzed, only two different dipole heights are used.

The dipoles are resonant ($\lambda/2$) or smaller which has a high influence on the efficiency but a small influence on the radiation pattern[21] of the dipole. For this theoretical study the efficiency is of limited importance since the PA distributions are compared qualitatively.

When evaluating the obtained predictions we faced the common problem of the inability to define the quality of a hyperthermia treatment[27]. From a biological point of view the focus is on thermal dose relationship[28,29] . Such an approach is well validated in a clinical environment although it provides only retrospective information. For applicator development, the main source of information are data from predicted specific absorption rate (SAR), or PA, distributions (where the PA and SAR values are related through the mass density). As a result, a strong need exists for an objective criterion to express the quality of the SAR distribution. The Effective Field Size (EFS[3]) and penetration depth as defined within the ESHO quality guidelines[30] provide a general solution for single applicators and SAR distributions in 'semi' homogenous, e.g. layered, phantoms. Other parameters, like the areas enclosed by the 25%, 75% iso-SAR contour and their ratio EFS75%/EFS25%[31,32] have been suggested for superficial hyperthermia. Here again, they are intended for use in simple phantom configurations. In the development of loco-regional (deep) hyperthermia techniques, application of EM-modelling has a longer history and various evaluation procedures have been used[33,34]. As a global indicator the ratio of the SAR50% in the tumour to SAR50% in the total volume is frequently used[15]. The aPA ratio follows an approach similar to that of Paulsen *et al.*[34]. It differs from the index defined by Wust *et al.*[15] in the sense that the quotient of power absorption in the target region and the neck is used, thus the influence of a normalization procedure is excluded. The aPA ratio is strongly dependent on the size of the target volume and thus the choice of its dimensions is of high importance. The size of the target region is chosen to vary from 2x2x2 cm to 8x8x8 cm, where the focus is on sizes between 4x4x4 cm and 6x6x6 cm since the aim is to heat advanced tumours together with lymph node metastases.

In this study, to speed up the analysis, we omitted SAR pattern optimization. Because the set-up under study is fairly symmetrical, we assumed that optimization of the amplitudes and phases would only minimally alter the SAR patterns. Further, we have focussed on the global PA pattern and therefore we have not performed a comparison of the set-ups in terms of (the avoidance of) hotspots in normal tissue. Therefore, we expect that the conclusions will hold when analyzing optimized SAR patterns.

4.2 Discussion of the results

For the positioning of the sources, we found that antenna positions close to the chin region should be avoided in order to decrease the influence of the limiting hotspot in the chin region. The optimal amount of antennas of the investigated set-ups is sixteen, where six and eight antennas are found to be highly suitable as well. The good performance with eight antennas as found in this study is in agreement with Jouvie *et al.*[35]. They found that a set-up comprising eight dipoles at 433 MHz for H&N HT is approximately optimal; their approach though was by use of 2D calculations. The number of antennas, however, should be increased when the frequency is increased, for an optimal SAR distribution[34]. More antennas, though, result in a higher complexity. For the clinical practice,

[3]EFS: the area enclosed by the 50% iso-SAR contour.

a system with low complexity is preferable and therefore a low amount of antennas is desired. For the frequency investigation we selected eight antennas since this provides a close to optimal result and is a clinically acceptable amount of elements.

For a set-up of eight antenna elements, it is found that low frequencies (100 MHz and 144 MHz) result in superficial absorbtion only (Figure 4). This seems very counter intuitive as lower frequencies generally correspond to higher penetration depths. At these frequencies for our set-up, a difficult complex interaction occurs between tissue and antennas. From the current results we anticipate that the interference pattern suffers from an insufficient distance between the antennas and the center of the anatomy. A small distance in terms of effective wavelength in the media may flatten the maximum and increases patient load influences.

The optimal frequency is amongst others dependent on the number and location of the sources and the target size. Hence, it is difficult to select a single optimal frequency. For target sizes between 4x4x4 cm and 6x6x6 cm optimal frequencies in the range of 400-600 MHz are found. For two out of three target sizes the best performance is obtained at 433 MHz where for the smallest target size at 550 MHz the best performance is achieved by use of the eight antenna set-up. For larger target sizes the optimal frequency range shifts to somewhat lower frequencies, i.e. between 300 MHz and 433 MHz.

This investigation was carried out using a 9.7 cm in diameter neck and scaled versions with neck diameters of 12 and 13.5 cm. The calculations at 300, 433 and 550 MHz indicate the best performance at 433 MHz for all realistic neck dimensions. It should be noted that usually a small neck contains more muscle in comparison to a large (in diameter) neck. A higher percentage of muscle results in a lower penetration depth thus reducing the interference at depth. Therefore a more pronounced focus is anticipated for a large neck with a high fat percentage. Jacobson and Melandsø[20] and Gross *et al.*[36] previously investigated the possibility to heat H&N tumours.

Jacobson and Melandsø predicted and measured a central focus in a cylindrical, muscle equivalent, phantom with four spiral antennas radiating with equal phases at 488 MHz. In the study of Gross *et al.*, four in-phase dielectric loaded circular horn antennas are used to illuminate a muscle phantom. They measured a better focus at 400 MHz compared to 915 MHz in case of a phantom with a diameter of 11 cm. The data as presented in this publication narrows down the range of interesting frequencies indicated by Jacobson and Melandsø but presents a confirmation by 3D FDTD calculations of the measurements by Gross *et al.*.

The influence of using multiple antenna rings is investigated by both Seebass *et al.*[37] and Paulsen *et al.*[34] who found an optimal frequency of approximately 150 MHz for their deep hyperthermia systems consisting of three (Seebass *et al.*) or four (Paulsen *et al.*) rings of antennas. Both studies differ from the present study in the fact that the aim is to heat tumours in the pelvic region where the average diameter of the body is approximately three times larger. Converting the optimal frequency for deep hyperthermia (150 MHz) to our set-up, taking into account the different required penetration depths and assuming a cylindrical approximation in both cases, would result in an optimal frequency around 450 MHz. This provides some support of an optimum frequency in the range of 400 to 600 MHz for heating head and neck tumours when using multiple antenna rings.

5 Conclusion

In this study, we investigated the ability of a multi-element, single antenna ring, H&N HT applicator to deposit RF energy selectively in the center of the neck, while sparing the normal tissue in the neck. It provides a quantitative confirmation of our intuitive applicator design.

It has been found that positioning antennas closely to the chin should be avoided. Further, eight antenna elements is shown to be a suitable number of antennas for frequencies in the investigated frequency band for a set-up of one concentric ring of equally spaced antennas. The optimum frequencies are shown to be in the frequency band between 400 and 600 MHz for the investigated target sizes. This frequency band shifts downwards for larger target volumes.

From the findings of this study and the fact that 433 MHz is an ISM frequency at which high power amplifiers are available in our clinic we feel it is highly justified to continue our investigations at 433 MHz. The actual number of antennas and use of multiple rings of antennas are subject of further research, where an optimum is expected around six to eight antennas per ring.

Acknowledgements

This work was financially supported by the Dutch Cancer Society, grant: DDHK 2003-2855. The authors further would like to thank J. Mooibroek for his contributions.

References

1. VA Marcial and TF Pajak. Radiation therapy alone or in combination with surgery in head and neck cancer. *Cancer*, 55:2259–2265, 1989.
2. RR Million and NJ Cassisi. *Management of head and neck cancer: a multidisciplinary approach.* JB Lippincott, New York, 1994.
3. S Dische, M Saunders, A Barrett, A Harvey, D Gibson, and M Parmar. A randomised multicentre trial of CHART versus conventional radiotherapy in head and neck cancer. *Radiother Oncol*, 37:123–126, 1997.
4. J-C Horiot, P Bontemps, W Van den Bogaert, R Le Fur, D Van den Weijngaert, M Bolla, J Bernier, A Lusinchi, M Stuschke, J Lopez-Torrecilla, AC Begg, M Pierart, and L Collette. Accelerated fractionation compared to conventional fractionation improves loco-regional control in radiotherapy of advanced head and neck cancers: Results of the EORTC 22851 randomized trial. *Radiother Oncol*, 44:111–121, 1997.
5. W Van den Bogaert, E Van Schueren, J-C Horiot, M De Vilhena, S Schraub, V Svoboda, G Arcangeli, M De Pauw, and M Van Glabbeke. The EORTC randomized trial on three fractions per day and misonidazole (trial no. 22811) in advanced head and neck cancer; long-term results and side effects. *Radiother Oncol*, 35:91–99, 1995.
6. JP Pignon, J Bourhis, and Designe L Domenge, C. Chemotherapy added to locoregional treatment for head and neck squamous-cel carcinoma: three meta-analyses of updated individual data. *Lancet*, 355:949–955, 2000.

7. A Trotti. Toxicity in head and neck cancer: a review of trends and issues. *Int J Rad Oncol Biol Phys*, 47:1–12, 2000.
8. S El-Sayed and N Nelson. Adjuvant and adjunctive chemotherapy in the management of squamous cell carcinoma of the head and neck region: A meta-analysis of prospective and randomized trials. *J Clin Oncol*, 14:838–847, 1996.
9. J Bernier, J Denekamp, A Rojas, E Minatel, J Horiot, H Hamers, P Antognoni, O Dahl, P Richaud, M Van Glabbeke, and M Pi. ARCON: Accelerated Radiotherapy with Carbogen and Nicotinamide in head and neck squamous cell carcinomas. the experience of the cooperative group of radiotherapy of the european organization for research and treatment of cancer (EORTC). *Radiother Oncol*, 55:111–119, 2000.
10. J Van der Zee. Heating the patient: a promising approach? *Ann Onc*, 13:1173–1184, 2002.
11. R Valdagni and M Amichetti. Report of long-term follow-up in a randomized trial comparing radiation therapy and radiation therapy plus hyperthermia to metastatic lymph nodes in stage IV head and neck patients. *Int J Rad Oncol Biol Phys*, 28:163–169, 1993.
12. R Valdagni, F-F Liu, and S Kapp. Important prognostic factors influencing outcome of combined radiation and hyperthermia. *Int J Rad Oncol Biol Phys*, 15:959–972, 1988.
13. M Amichetti, M Romano, L Busana, A Bolner, G Fellin, G Pani, L Tomio, and R Valdagni. Hyperfractionated radiation in combination with local hyperthermia in the treatment of advanced squamous cell carcinoma of the head and neck: a phase I-II study. *Radiother Oncol*, 45:155–158, 1997.
14. M Serin, HS Erkal, and A Cakmak. Radiation therapy, cisplatin, and hyperthermia in combination in management of patients with recurrent carcinomas of the head and neck with meta-static cervical lymph nodes. *Int J Hyperthermia*, 15:371–381, 1999.
15. P Wust, M Seebas, J Nadobny, P Deuflhard, G Mönich, and R Felix. Simulation studies promote technological development of radiofrequency phased array hyperthermia. *Int J Hyperthermia*, 12:477–498, 1996.
16. R Ben-Yosef and DS Kapp. Direct clinical comparison of ultrasound and radiative electromagnetic hyperthermia in the same tumours. *Int J Hyperthermia*, 11:1–10, 1995.
17. RL Magin and AF Peterson. Noninvasive microwave phased arrays for local hyperthermia: a review. *Int J Hyperthermia*, 5:429–450, 1989.
18. MM Paulides, DHM Wielheesen, J Van der Zee, and GC Van Rhoon. Assessment of the local SAR distortion by major anatomical structures in a cylindrical neck phantom. *Int J Hyperthermia*, 21:382–400, 2005.
19. FM Henke, WT Joines, and TV Samulski. Variations of focal regions versus number and positions of sources in two-dimensional media. *Int J Hyperthermia*, 17:382–400, 2001.
20. S Jacobsen and F Melandsø. The concept of using multifrequency energy transmission to reduce hot-spots during deep-body hyperthermia. *Ann Biom Eng*, 30:1–10, 2002.
21. CA Balanis. *Antenna theory: Analysis and design.* John Wiley & Sons, Inc., New York, 2nd edition edition, 1997.

22. CHM Clemens, SHJA Vossen, AB Woltering, and APM Zwamborn. Study of the possible effects on health of the use of portable terminals within the C2000 radio network. TNO-FEL internal report: FEL-02-C152, Reproduction Department of The Netherlands Organisation of Applied Scientific Research (TNO), 2003.
23. A Taflove and SC Hagness. *Computational Electrodynamics: The Finite-Difference Time-Domain Method.* Artech House, 685 Canton Street, Norwood, MA 02062, 3rd edition, 2005.
24. G Mur. Absorbing boundary conditions for the finite-difference approximation of the time-domain electromagnetic field equations. *IEEE Trans Electromag Compat*, 23:377–382, 1981.
25. The Nello Carrara Institute of Applied Physics of the Consiglio Nazionale delle Ricerche (IFAC-CNR). Florence. Italy. http://niremf.ifac.cnr.it/tissprop/. 1997-2002.
26. S Gabriel, RW Lau, and C Gabriel. The dielectric properties of biological tissues III: Parametric models for the dielectric spectrum of tissues. *Phys Med Biol*, 41:2271–2293, 1996.
27. JR Oleson. If we cant define the quality, can we assure it? *J Rad Oncol Biol Phys*, 16:879, 1989.
28. O Dahl, R Dalene, BC Schem, and O Mella. Status of clinical hyperthermia. *Acta Oncol*, 38:863–873, 1999.
29. MW Dewhirst, L Pronnitz, D Thrall, D Prescott, S Clegg, C Charles, J MacFall, G Rosner, T Samulski, E Gillette, and S LaRue. Hyperthermia treatment of malignant diseases: Current status and a view towards the future. *Semin Oncol*, 24:616–625, 1997.
30. JW Hand, JJW Lagendijk, Bach Andersen J, and JC Bolomey. Quality assurance guidelines for ESHO protocols. *Int J Hyperthermia*, 5:421–428, 1989.
31. EA Gelvich, VN Mazokhin, and II Throshin. An attempt at quantitative specification of SAR distribution homogeneity. *Int J Hyperthermia*, 12:431–436, 1996.
32. PMJ Rietveld, JB Van de Kamer, J Van der Zee, and et al. Influence of variations in position, form, and contents of semi-simple phantoms in the BSD-2000 Sigma-60 applicator on SAR distributions. In *Abstracts of the International Congress of Hyperthermic Oncology (ICHO-2000)*, page 145, Kyongju, South Korea, April 26^{th}-29^{th} 2000.
33. SN Hornsleth. *Radiofrequency regional hyperthermia.* PhD thesis, Aalborg University, Denmark, 1996.
34. KD Paulsen, S Geimer, J Tang, and WE Boyse. Optimisation of pelvic heating rate distributions with electromagnetic phased arrays. *Int J Hyperthermia*, 15:157–186, 1999.
35. F Jouvie, JC Bolomey, and G Gaboriaud. Discussion of the capabilities of microwave phased arrays for hyperthermia treatment of neck tumours. *IEEE Trans Micr Theor Tech*, 34:495–501, 1986.
36. EJ Gross, TC Ceetas, PR Stauffer, RL Liu, and ML Lumori. Experimental assessment of phased-array heating of neck tumours. *Int J Hyperthermia*, 6:454–474, 1990.
37. M Seebass, R Beck, J Gellerman, J Nadobny, and P Wust. Electromagnetic phased arrays for regional hyperthermia: Optimal frequency and antenna arrangement. *Int J Hyperthermia*, 17:321–336, 2001.